Materials Science & Engineering A 700 (2017) 512–518

Contents lists available at ScienceDirect

Materials Science & Engineering A

journal homepage: www.elsevier.com/locate/msea

Microstructure evolution and embrittlement of electron beam welded TZM alloy joint

Yongyun Zhang[a], Ting Wang[a,b,*], Siyuan Jiang[a], Binggang Zhang[b], Yong Wang[c], Jicai Feng[a,b]

[a] *Harbin Institute of Technology at Weihai, Shandong Provincial Key Laboratory of Special Welding Technology, Weihai 264209, China*
[b] *State Key Laboratory of Advanced Welding and Joining, Harbin Institute of Technology, Harbin 150001, China*
[c] *Shanghai Xinli Power Equipment Research Institute, Shanghai 201109*

ARTICLE INFO

Keywords:
Electron beam welding
TZM alloy
Microstructure
Precipitates
Mechanical properties

ABSTRACT

To investigate the influence of microstructure evolution on mechanical properties of a molybdenum-titanium-zirconium (TZM) alloy joint welded by electron beam welding (EBW), detailed microstructure of the joint was examined by electron backscatter diffraction (EBSD) and transmission electron microscopy (TEM). The microhardness of the cross section was measured and tensile strengths at temperatures of 293 K as well as 1273 K were tested. The crystallized grains of weld zone (WZ) were coarsened severely, but the dispersed distribution of Mo_2C and ZrO_2 particles inside grains caused the microhardness of WZ to be higher than that of heat affected zone (HAZ). MoO_2 and TiO_2 precipitates easily segregated on grain boundaries due to microsegregation. Since the large differences in the interatomic distance between Mo/MoO_2 and Mo/TiO_2, the precipitates segregated on grain boundaries and Mo matrix were deemed to be incoherent. Thus, tensile strength of the welded joint was just 50% of that of base metal and the elongation was nearly decreased to zero with a brittle fracture mode.

1. Introduction

Molybdenum-based alloys are desired for many high-temperature applications due to excellent mechanical properties at high temperature as well as thermal shock resistance [1–3]. Furthermore, with the development of aerospace and nuclear industries, Mo-based alloys are increasingly demanded to obtain higher mechanical properties at different temperature ranges in these industries. Moreover, TZM alloy, with excellent tensile strength at high temperature due to the addition of a small amount of Ti and Zr as well as C, becomes more popular refractory metal material with unexceptionable application prospects [4–7]. Hence, the joining of TZM has been paid increasing attentions from researchers.

Researches on the joining of Mo-based alloys had been studied, such as friction stir welding [8], brazing [9,10] and so on. However, the application of solid state joining in industrial manufacture was enslaved to its intricate welding technology [11]. On the other hand, brazing joints with poor fatigue performance limited their applications in industrial production. The welding process of TZM should be conducted with high welding heat input owing to the high melting point of TZM. Hence, fusion welding methods were taken into account. Some researches on the welding of Mo-based alloys by argon arc welding had been declared in recent years. Miller et al. illustrated that the addition of C, B and Zr to molybdenum could improve the ductility of the joints by gas-tungsten arc welding. Moreover, atom probe tomography was performed to reveal that the segregation of alloying elements would deplete oxygen and nitrogen at grain boundaries, and then restrained intergranular fracture of the joints [12]. In addition, Tabernig et al. exemplified that the protection of argon could not eliminate the impact of oxygen, which would result in the loss of mechanical properties, on the weld metal [13].

EBW was suitable for the welding of refractory metal due to its vacuum atmosphere and extreme energy density [14–16]. A number of investigations into Mo-based alloy joints welded by EBW had been documented. Wadsworth et al. found that the tensile strength of the TZM welded joint by EBW was higher than other joints welded by LW and TIG on account of the smaller grain size in EB-weld zone [17]. Chatterjee et al. informed that the loss of ductility was attributed to the formation of Mo-oxide instead of the consequent work hardening in FZ [18]. Cockeram et al. considered that the concentration of carbon and boron could replace the enrichment of oxygen on the grain boundaries, which can reduce the brittleness of joint [19]. However, the qualitative analyses of these oxides, produced in the welding process, have not been mentioned among these studies. Moreover, the influencing mechanism of segregation of oxygen element on grain boundaries as well as the mechanical properties of these joints at the high-temperature had

---

[*] Correspondence to: Shandong Provincial Key Laboratory of Special Welding Technology, Harbin Institute of Technology at Weihai, Wenhua West Road, Weihai 264209, China.
E-mail address: fgwangting@163.com (T. Wang).

http://dx.doi.org/10.1016/j.msea.2017.05.076
Received 23 April 2017; Received in revised form 19 May 2017; Accepted 20 May 2017

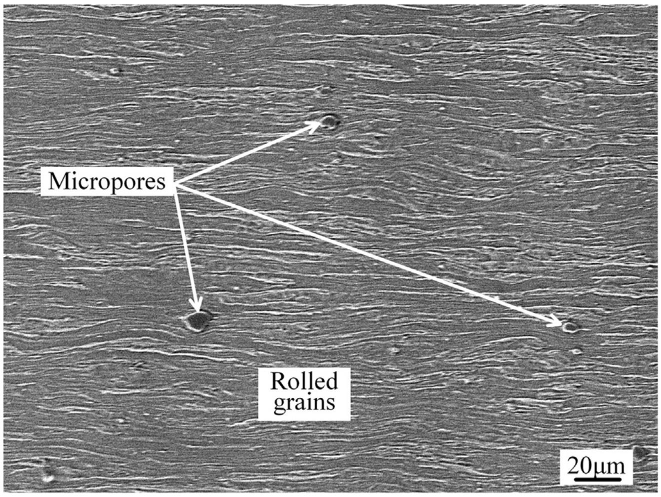

Fig. 1. Elongated grain structure of TZM alloy.

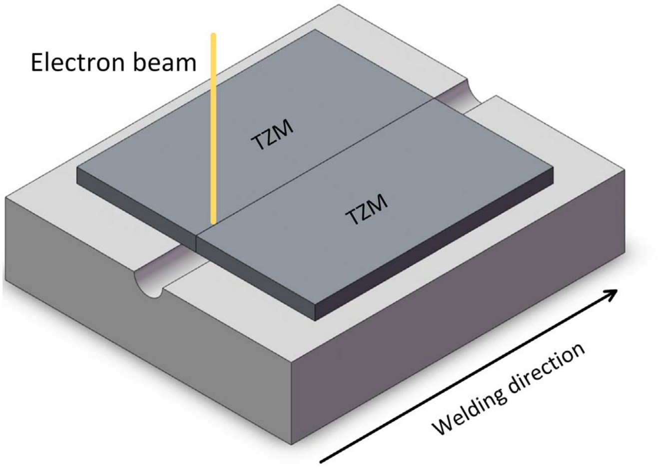

Fig. 2. Schematic illustration of EBW process.

been rarely reported. Hence, the studies on the reactions of the alloying elements during the welding process and the influence of the distribution of precipitates on mechanical properties of the joint are important to be investigated.

In this study, EBW experiments of TZM alloy butt welding joint in vacuum environment were conducted. Detailed microstructural investigations into different weld regions were discussed. The tensile strengths under normal temperature (293 K) and high-temperature (1273 K) were measured, and the fracture graphs were collected in SEM. Analyses of grain orientation and phase distribution were examined by orientation imaging microscopy. The transgranular and intergranular precipitates were identified by TEM images with selected-area diffraction patterns.

2. Experimental

In this experiment, EBW was carried out to join TZM alloy plates with a dimension of 100 × 25 × 3.0 mm produced by powder metallurgy method. The microstructure of base metal (BM) was composed of hot-rolled elongated grains shown in Fig. 1. The chemical composition of TZM was listed in Table 1. The base metal was cleaned before welding by mechanically and chemically methods. The schematic diagram of a butt welded joint was displayed in Fig. 2. The welding process was undertaken by EBW equipment under the vacuum degree of 4×10^{-2} Pa and at an accelerating voltage of 70 kV, a beam current of 35 mA as well as a welding speed of 350 mm/min.

The welded joints were sliced by wire-cut electric discharge machine for the preparation of the metallographic and tensile specimens. The metallographic specimens were sanded by abrasive paper, then polished and etched in a reagent of 50 mL HNO_3, 30 mL H_2SO_4 and 30 mL H_2O. The microstructure was observed by optical microscope (OLYMPUS DSX-510) and scanning electron microscopy (Zeiss MERLIN Compact) with electron backscattering diffraction (EBSD) system. EBSD-OIM-attached Digiview 5 was used to get orientation and phase maps of the joint-(WZ, FZ, HAZ and BM) and the typical step size was kept as 1 μm. As for EBSD analysis, the specimens were prepared by electropolishing in the reagent of $CH_3OH + H_2SO_4$ in 9:1 (in volume ratio) at a voltage of 20 V and the time of 10 s. The microhardness distribution along horizontal direction of the joint cross section was evaluated by Vickers microhardness tester (HV-1000-DT) at the load of 200 g and dwell time of 10 s. The tensile tests were carried out with the universal electronic material testing machine (Instron 2382) at a displacement velocity of 1 mm/min. The fracture surfaces of the welded joint and BM were observed by SEM. The micrographs of WZ and BM were investigated by transmission electron microscope (JEOL-2100).

Table 1
Chemical composition of TZM alloy (mass fraction,%).

Ti	Zr	C	Mo
0.50	0.08	0.02	Bal.

3. Results and discussion

3.1. Microstructure of the joint

Owning to the uneven temperature fields in the depth direction of the joint [16] caused by the strong penetration power and high energy density of electron beam [14,15], the weld zone looked like the “bell” shape as presented at Fig. 3(a). On account of different microstructures in the welded joint, all the four distinct regions of the weld zone (WZ), fusion zone (FZ), heat affected zone (HAZ) and BM were clearly observed in Fig. 3(a). Welding pores gathered on the grain boundaries of WZ were also clearly displayed in Fig. 3(a), and the formation of welding pores would be detailedly discussed in the context. The microstructures in different regions of the joint obtained by EBSD were displayed in Fig. 3(b)–(e). It was easy to find that four regions were clearly distinguished from these micrographs due to the changes in grain orientations and crystallite dimensions, which could provide further proof for the consequences of microstructure in OM. Fig. 3(b) revealed that the crystal seriously grew up in WZ. As Fig. 3(c) conveyed that columnar grain in FZ was produced and the growth direction of columnar crystal was perpendicular to the fusion line. Grain size charts of the different regions collected by OIM software for EBSD analysis were displayed in Fig. 4, which conveyed that grains in WZ had been coarsened severely due to the high temperature of the molten pool. As well, the average grain size in WZ was 60 μm in this paper, which was far more than that of HAZ and BM. The average grain size of HAZ and BM counted by OIM analysis was 15.6 μm and 4.5 μm, respectively. Due to the affection of the weld thermal cycle, rolled grains recrystallized in HAZ and the grain size obviously increased. However, crystals did not completely recrystallize at the BM-HAZ interface because of low growth driving force.

3.2. The analysis of the precipitates

3.2.1. Distributions of precipitates

To investigate contents of distinct phases in different zones, the microstructures of WZ and HAZ contained information of image quality and phase distribution in EBSD analysis were shown in Fig. 5(a) and (b), respectively. Fig. 5(a) illustrated that the cubic molybdenum